

Late Cenozoic transtensional fault belt discovered on the boundary of the Awati Sag in the northwestern Tarim Basin

Yue-Jun Li · Qiang Zhang · Guang-Ya Zhang ·
Hai-Jun Yang · Xian-Zhang Yang · Jun Shi ·
Yuan Neng · Yan-Gui Chen · Lei Wen

Received: 27 September 2014 / Accepted: 17 January 2015 / Published online: 28 January 2015
© Springer-Verlag Berlin Heidelberg 2015

Abstract Late Cenozoic transtensional fault belt was discovered on Shajingzi fault belt, NW boundary of the Awati Sag in the northwestern Tarim Basin. And numerous Quaternary normal faults were discovered on Aqia and Tumuxiuke fault belts, SW boundary of Awati. This discovery reveals Quaternary normal fault activity in the Tarim Basin for the first time. It is also a new discovery in the southern flank of Tianshan Mountains. Shajingzi transtensional fault belt is made up of numerous, small normal faults. Horizontally, the normal faults are arranged in right-step, en echelon patterns along the preexisting Shajingzi basement fault, forming a sinistral transtensional normal fault belt. In profile, they cut through the Paleozoic to the mid-Quaternary and combine to form negative flower structures. The Late Cenozoic normal faults on the SW boundary of Awati Sag were distributed mainly in the uplift side of the preexisting Aqia and Tumuxiuke basement-involved faults, and combined to form small horst and graben structures in profile. Based on the intensive seismic interpretation, careful fault mapping, and growth index analysis, we conclude that the normal fault activity of Shajingzi transtensional fault belt began from Late Pliocene and ceased in Late Pleistocene (mid-Quaternary). And the normal faulting on the SW boundary of Awati Sag began from the very beginning of

Quaternary and ceased in Pleistocene. The normal faulting on Awati's SW boundary began a little later than those on the NW boundary. The origin of Shajingzi transtensional normal fault belt was due to the left-lateral strike-slip occurred in the southern flank of Tianshan, and then, due to the eastward escape of the Awati block, a tensional stress developed the normal faults on its SW boundary.

Keywords Pliocene–Pleistocene normal fault · Late Cenozoic transtensional normal fault belt · Left-lateral strike-slip · Awati Sag · Northwestern Tarim Basin · Southern flank of Tianshan Mountains · Seismic interpretation

Introduction

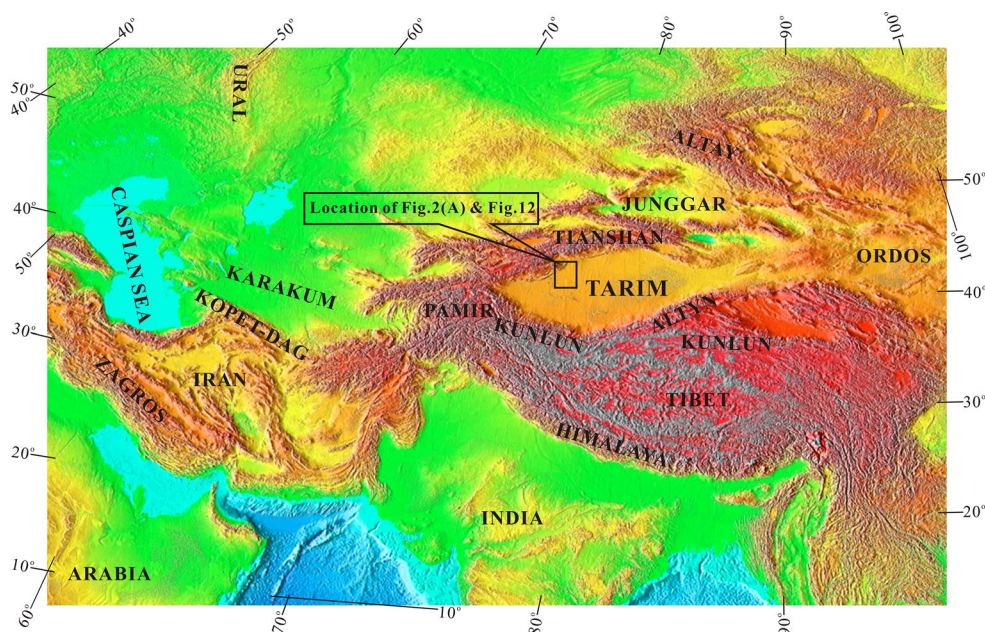
Tarim Basin surrounded by Tianshan, Kunlun, and Altyn Mountains is one of the largest Meso-Cenozoic sedimentary basins in central Asia (Fig. 1). Under the far-field effect of India–Asia collision, Cenozoic compressional structures are abnormally developed in central Asia accompanying with the mountain building (Molnar and Tapponnier 1975; Tapponnier and Molnar 1977; Tapponnier et al. 1986; Windley et al. 1990; Guo et al. 1992; Allen et al. 1993; Avouac and Tapponnier 1993; Zhang et al. 1996; Sobel and Dumitru 1997; Li et al. 2001; Shu, et al. 2003; Charreau et al. 2006, 2009). Typical Cenozoic thrust belts are developed on the northern margin of Tarim Basin (Lu et al. 1994, 2000; Allen et al. 1999; Sun et al. 2002; Schärer et al. 2004; Tang et al. 2004; Guan et al. 2007; Wang et al. 2009; Yang et al. 2010), where this is also the southern piedmont of Tianshan. Beside the compressional structures, some Cenozoic strike-slip tectonics and normal fault structures have been identified out in Tianshan Mountains and

Y.-J. Li · Q. Zhang (✉) · L. Wen
Institute of Geology and Geophysics, Chinese Academy
of Sciences, Beijing 100029, China
e-mail: Zhangqiangfendou@126.com

G.-Y. Zhang
Research Institute of Petroleum Exploration and Development,
PetroChina, Beijing 100083, China

H.-J. Yang · X.-Z. Yang · J. Shi · Y. Neng · Y.-G. Chen
Tarim Oilfield Company, PetroChina, Korla 841000, China

Fig. 1 Location of Tarim Basin and the studied area



its adjacent area (Avouac and Tapponnier 1993; Charreau et al. 2006, 2009; Zhao et al. 2012; Li et al. 2013). These tectonics and structures are important for the correct understanding the mountain-building process and the far-field effect of the India–Asia collision.

Many valuable geological information for Tianshan tectonics is preserved in the northern margin of Tarim Basin, where it is covered by modern deposits and impossible for the geologist to observe directly. Recent developments in seismic exploration technology and the enrichment of seismic exploration data have enabled the gradual discovery and study of Meso–Cenozoic extensional structures in the Tarim Basin (Tang et al. 1999; Tang and Jin 2000; Zhang et al. 1999; Jia et al. 2001; Wei et al. 2001; Chen et al. 2009; Zhao et al. 2012; Qi et al. 2012; Li et al. 2013).

Jurassic extensional structures were discovered earlier and are believed to be part of the North Tethys Mesozoic extensional structures (Jia et al. 2001; Chen et al. 2009) or a result of post-orogeny stress relaxation of the South Tianshan (Zhao et al. 2012; Li et al. 2013). Formerly, Cenozoic normal faults were thought to be distributed only on the Yaha and Luntai fault belts in the North Tarim Rise. These normal faults are superimposed onto older, underlying thrust faults and form negative inversion structures (Tang et al. 1999; Tang and Jin 2000; Zhang et al. 1999; Wei et al. 2001). Recent studies have revealed numerous Cenozoic normal faults widespread in Tabei Rise. These normal faults are usually arranged in en echelon patterns and form transtensional fault belts. These transtensional fault belts exhibit the far-field effect of India–Asia collision (Zhao et al. 2012; Li et al. 2013).

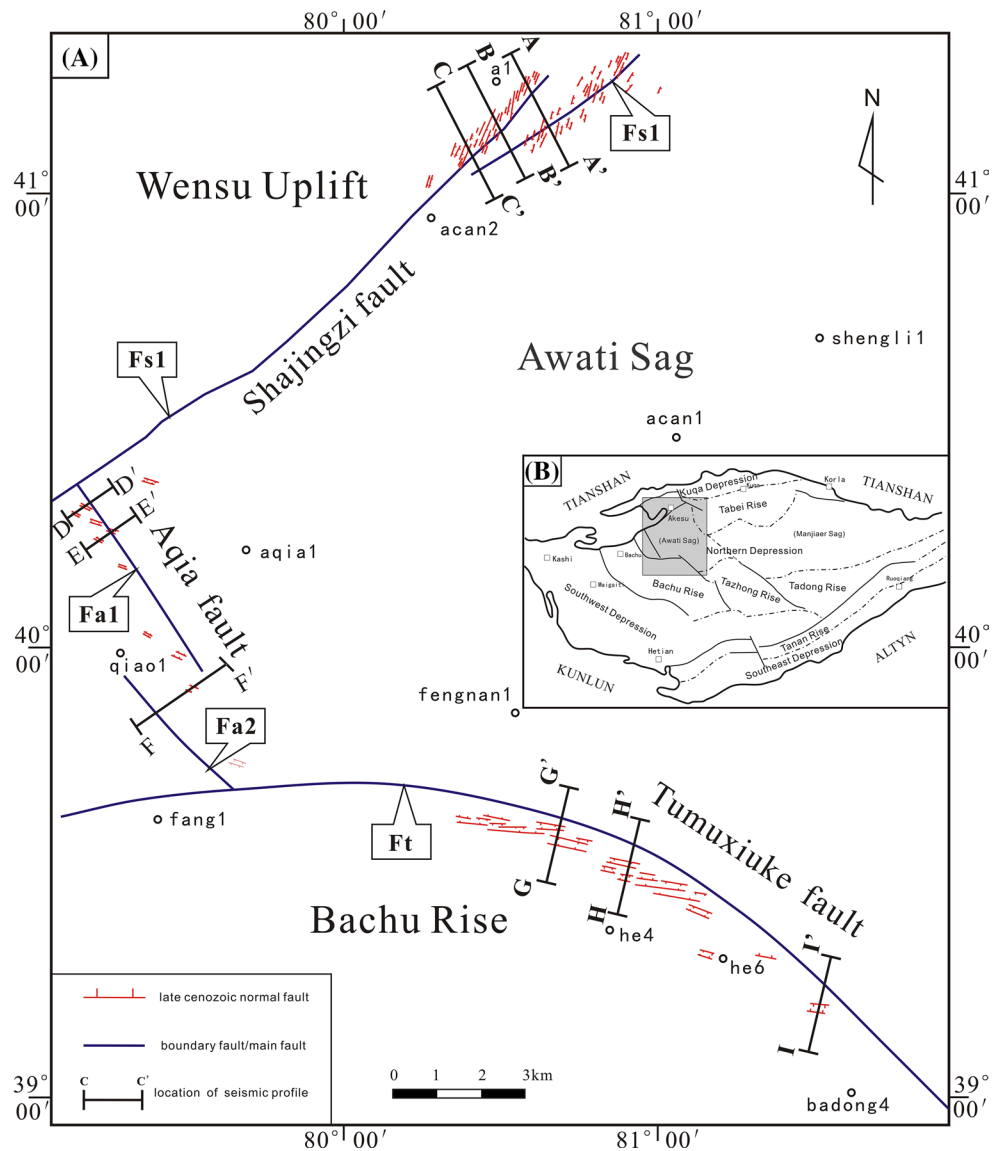
By continuing the study of Cenozoic extensive structures westward, we have carefully interpret almost all the seismic profiles in and around the Awati Sag in recent years, and discovered Pliocene–Pleistocene normal faults on the Shajingzi, Tumuxiuke, and Aqia belts (Fig. 2). The normal faults on Shajingzi, NW boundary of Awati, were arranged in en echelon pattern, implying a left-lateral strike-slip in Pliocene–Pleistocene along Shajingzi belt. The normal faulting on Aqia and Tumuxiuke, SW boundary of Awati, occur in Early–Middle Quaternary, induced by the eastward escape of Awati. This is a new discovery of Late Cenozoic strike-slip fault belt in northern Tarim Basin or the southern piedmont of Tianshan, and also the first discovery of Quaternary normal fault activity in the Tarim Basin.

Late Cenozoic normal faults revealed around the Awati Sag

Seismic data are the foundation of this paper; therefore, a concise seismic stratigraphic chart of the Awati Sag and its adjacent areas (Table 1) is useful to better understand this study. Correlations of important seismic reflection surfaces with lithostratigraphic and chronostratigraphic units are based on the studies by Jia et al. (1992, 2004), Wang (1992), Li et al. (1992), and Zhang et al. (2004).

The Shajingzi, Aqia, and Tumuxiuke faults are three boundary faults located between the Awati Sag and its neighboring geological units. Late Cenozoic normal faults are revealed on all of these boundary faults (Fig. 2).

Fig. 2 Distribution of the Late Cenozoic normal faults around the Awati Sag. “Fs1” is the NW branch of Shajingzi fault, “Fs2” is the SE branch of Shajingzi fault, “Fa1” is the NE branch of Aqia fault, “Fa2” is the SW branch of Aqia fault, “Ft” is the Tumuxiuke fault (same in the following figures)



Late Cenozoic normal faults revealed on the Shajingzi belt

Late Cenozoic normal faults were first discovered on the Shajingzi fault. The normal faults are distributed on the northeastern segment of the Shajingzi fault, and the normal faulting was controlled by the preexisting basement-involved Shajingzi fault. The normal faults are grouped into right-step, en echelon patterns and form two transtensional normal fault belts (Fig. 2). A–A', B–B', and C–C' are three seismic profiles crossing the Shajingzi fault belt; we revealed Late Cenozoic normal faults on all these profiles (Figs. 2, 3, 4).

In the A–A' seismic profile (Figs. 2, 3), the Shajingzi basement-involved fault consists of northwestern and southeastern branches. The southeastern branch (Fs2) is derived from the northwestern branch (Fs1), which is the

main fault. Late Cenozoic normal faults were developed on both Fs1 and Fs2.

There are three Late Cenozoic normal faults on Fs2, two of them dip to the east and one to the west. These normal faults extend downward into the pre-Cenozoic layer and upward into the Quaternary deposit. Tb at the lower part of the Quaternary is the upmost reflection surface reached by the normal faults on Fs2. The normal faults in the pre-Cenozoic layers are unclear due to the preexisting basement-involved fault structures. In the Cenozoic, the fault displacements are equal at all the reflection surfaces in the lower part of the Kuqa Formation (strata between T3 and T2) and the sediments below it, indicating that the normal faulting began in Late Pliocene. From the upper part of Kuqa Formation, the displacements of the normal faults decrease gradually and disappear in the lower part of the Quaternary deposit. This indicates that the normal faulting

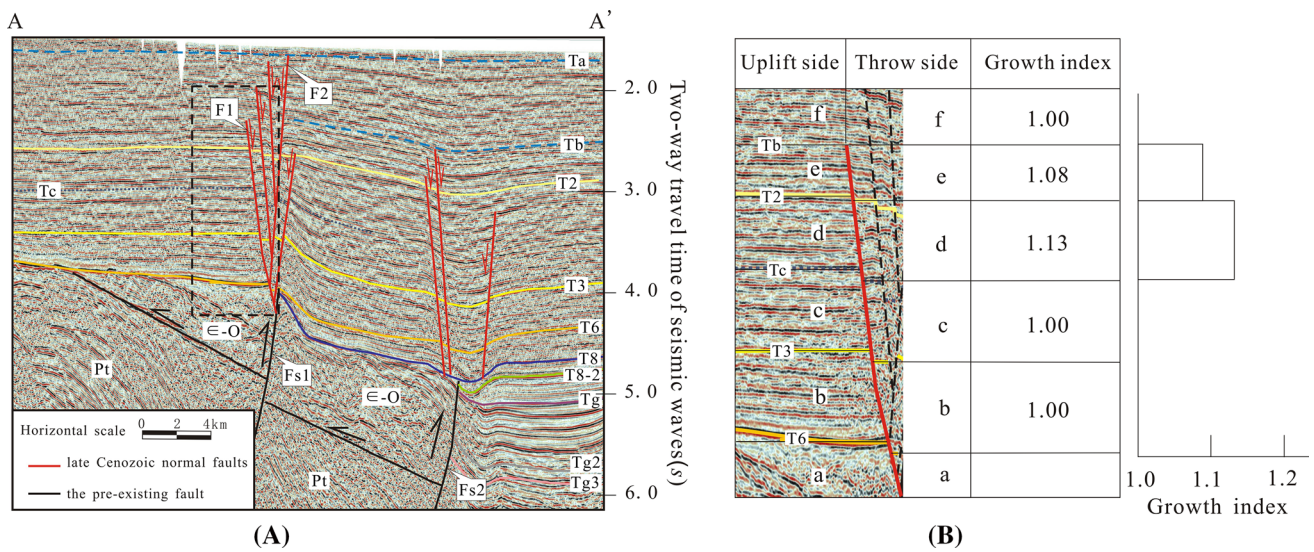


Fig. 3 A–A' seismic profile across the Shajingzi fault belt (see location in Fig. 2). **A** Seismic profile, **B** growth indices of the F1 fault: (a) pre-Mesozoic; (b) Miocene; (c) Lower Kuqa Formation; (d) Upper Kuqa Formation; (e) Lower Quaternary; (f) Middle–Upper Quaternary

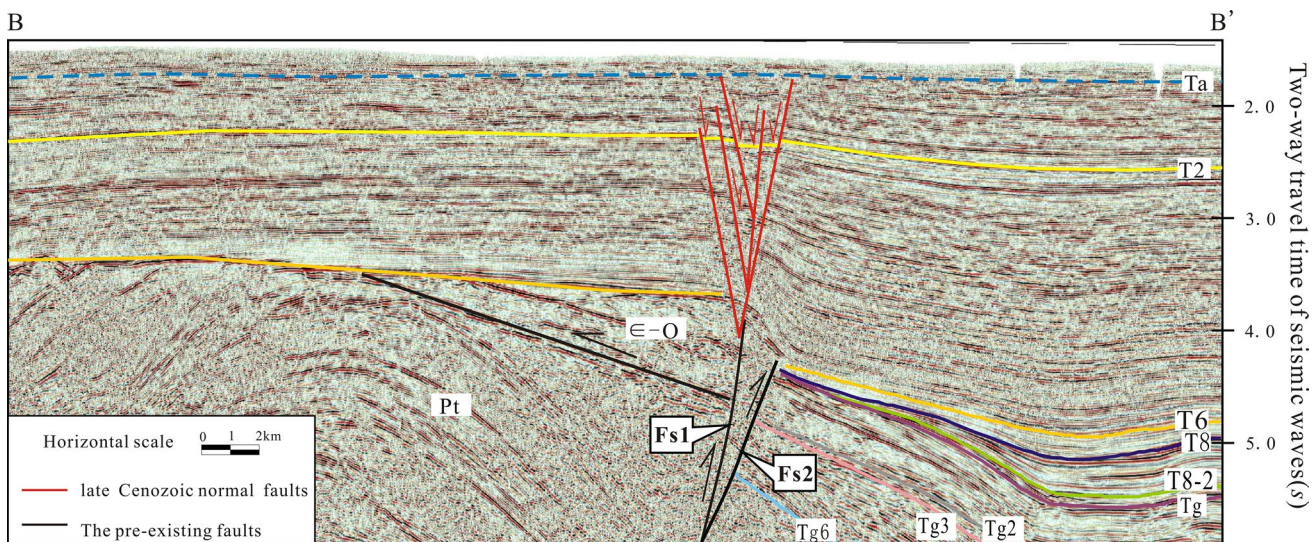


Fig. 4 B–B' seismic profile across the Shajingzi fault belt (see location in Fig. 2)

began in the Late Pliocene (the upper part of Kuqa Formation), lasted to Early Quaternary, and ceased thereafter. Owing to the small fault displacements, it is difficult to measure and calculate the growth index of the Late Cenozoic normal faults on Fs2.

Five Late Cenozoic normal faults were revealed on Fs1, which is the main Shajingzi fault. In profile, two of the faults are directed to the northwest and three to the southeast forming a small negative flower structure. The normal faults extend downward into the pre-Cenozoic, where they become unclear due to preexisting fault structures. They cut through the T2 upward into the Quaternary deposits.

Their fault displacements gradually decrease and finally disappear at Ta, which is a seismic reflect surface in the upper part of Quaternary deposits, also the upmost reflect surface reached by the normal faults on Fs1. We use F1 on the left of the A–A' profile for an example of the growth index calculation to show the normal faulting process (Fig. 3B).

The growth index (Ei), based on the concept of growth strata and growth fault, is used to study the active process (i.e., growth) of the faults. It is a commonly used index to describe the formation and evolution of a fault, especially normal faults. It is defined as the ratio of the stratigraphic

unit thicknesses on the downthrown side (H1) to the unit thickness on the upthrown side (H2), i.e.,

$$E_i = H_1/H_2.$$

$E_i = 1$ indicates that the stratigraphic unit thicknesses on both sides of a fault are equal, and thus, the fault was not active during the deposition of the stratigraphic unit; $E_i > 1$ indicates that the stratigraphic unit thickness on the downthrown side is larger than that on the upthrown side and thus reveals that the fault was active during the deposition of the stratigraphic unit. Larger values of E_i correspond to stronger fault activity (Tang and Jin 2000; Wei et al. 2001; Li et al. 2013).

The upmost reflection surface reached by the F1 fault in the A–A' seismic profile is not the upmost surface reached by this normal fault belt. The Ta reflection surface reached by F2 is the upmost surface reached by this normal fault belt. The main purpose of calculating the growth index of the F1 fault was to show the beginning of the normal fault activity.

The Pliocene Kuqa Formation is divided into two parts by Tc, a seismic reflection surface in the middle of the Kuqa Formation. The fault displacements of the Tc reflection surface and those below it are identical; the thickness of corresponding sediments on both sides of F1 is equal, and the growth indices of all the layers below Tc are 1.00, indicating that the normal fault was not active before Tc. The fault displacements at the bottom of Quaternary (T2) are obviously smaller than those at the Tc reflection surface. The growth index of the upper part of the Kuqa Formation (sediment between T2 and Tc) is 1.13, indicating that the normal fault activity began at the Tc reflection surface. The F1 fault extends upward into the Quaternary through T2, after which the fault displacements continuously decrease and finally disappear in the lower part of the Quaternary deposits. The F1 fault does not cut through the middle-upper part of the Quaternary deposits. The growth index of the lower part of the Quaternary deposits is 1.08 and that of the middle-upper part is 1.00 (Fig. 2B).

Results from the growth index analyses show that the normal faulting on the Shajingzi belt began in Late Pliocene (late stage of the sedimentary history of the Kuqa Formation) and last to mid-Quaternary. The peak stage of the normal faulting ($E_i = 1.13$) may be in the Late Pliocene.

The B–B' seismic profile is located southwest of the A–A' profile (Figs. 2, 4), near the Shan'an 1 well. On this profile, the Shajingzi is one basement-involved fault. Its deriving branch (Fs2) was disappeared, and a Late Cenozoic normal fault belt was developed on it. The normal fault belt is similar to that of Fs1 of the A–A' profile. The normal fault belt is composed of five normal faults: two of them dip northwest, three of them dip southeast, and together they form a negative flower structure. The normal fault belt

extends downward into the pre-Cenozoic and upwards into the Quaternary, through T2. The upmost reflection surface reached by the normal faults is Ta, which is located in the middle-upper part of the Quaternary deposits. The seismic reflection in the normal fault belt is not clear enough to calculate the growth index. The origin and evolution process of normal fault activity is identical to that of the A–A' faults.

The C–C' seismic profiles are located near the southwest end of the Shajingzi normal fault belt (Figs. 2, 5). Four normal faults make up the belt (one dipping northwest and the others southeast) and together form a small asymmetric graben. Seismic reflection inside the normal fault belt is not clear enough to enable the calculation of the growth index of each individual normal fault. Therefore, we grouped them as a single fault (i.e., belt) to directly observe the fault displacement and analyze the normal faulting process.

The fault displacements of the Tb reflection surface, which is located in the middle of the Kuqa Formation and those below (displacements between b and b', c and c', d and d'), are equal (Fig. 5). Therefore, the stratigraphic thicknesses of the corresponding layers on the two sides of the fault (belt), below the Tb reflection surface, are equal, and the growth indices of each layer below Tc are 1.00, indicating that the normal faulting has not occurred before Tc. The fault displacement decreases gradually, upward from the Tb reflection surface, until reaching the Ta reflection surface. The normal faults do not cut through the Ta reflection surface and the sediments above it. This indicates that the normal faulting began in Late Pliocene (Tc), lasted to mid-Quaternary, and then ceased.

Late Cenozoic normal faults revealed on the Aqia belt

The Aqia fault consists of two basement-involved branches (east and west branches), dipping toward each other (Fig. 2). Late Cenozoic normal faults were revealed mainly between the two branches.

D–D' is a 2D seismic profile across the northern segment of the Aqia belt (Figs. 2, 6). Three normal faults were revealed on this profile. The left two normal faults dip toward each other and form a small graben structure. The normal faults cut downward into the Paleozoic and upward into the Quaternary through T2 reflection surfaces. The fault displacements decrease gradually upward from T2 and disappear at Ta reflect surface in middle-upper part of the Quaternary deposits. The left two normal faults extend downward into the Paleozoic directly through T2. T2 is a large hiatus from the Upper Permian to the Neogene and an even lower part of the Quaternary. We cannot accurately estimate the activation time of the normal faulting based on these two normal faults due to the whole lacuna

Fig. 5 C–C' seismic profile across the Shajingzi fault belt (see location in Fig. 2)

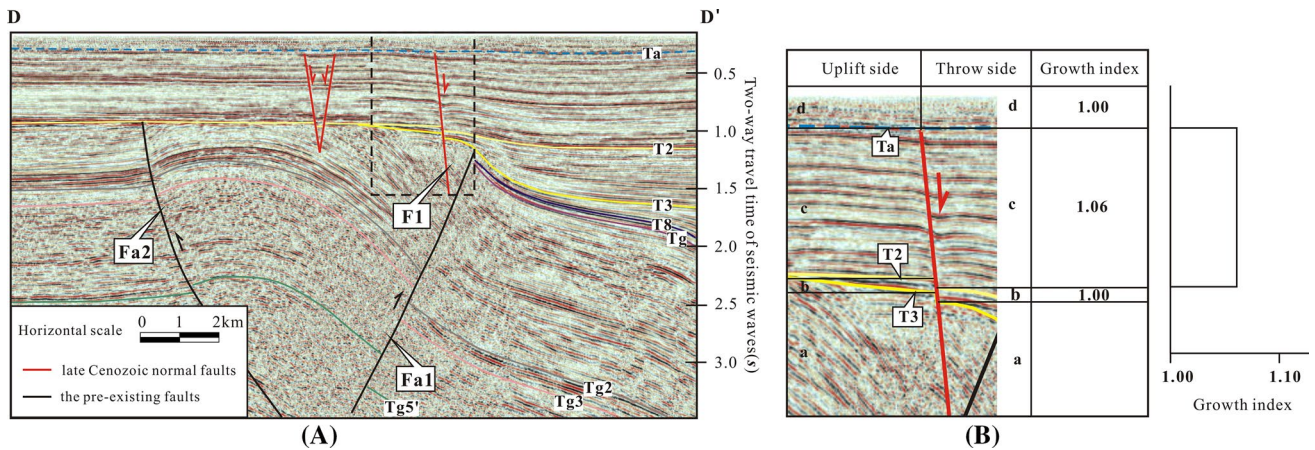
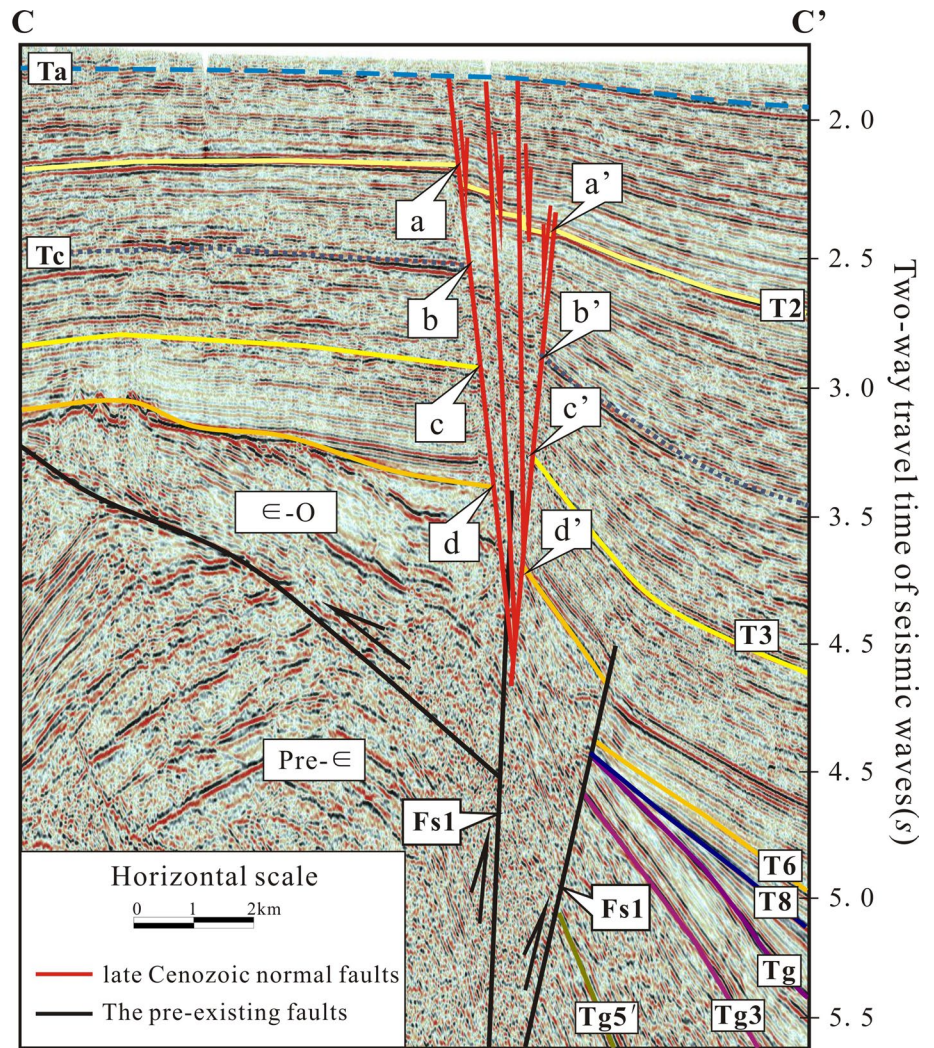


Fig. 6 D–D' seismic profile across the Aqia fault belt (see the location in Fig. 2). **A** Seismic profile, **B** growth indices of the F1 fault: (a) pre-Cenozoic; (b) Kuqa formation of Pliocene; (c) Middle–Lower Quaternary; (d) Upper Quaternary

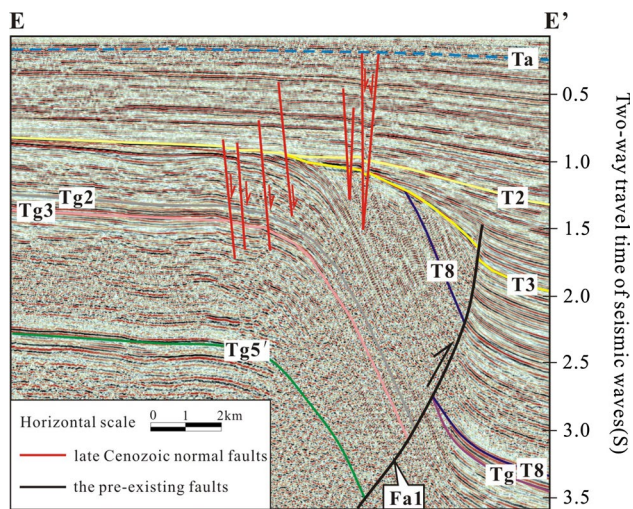


Fig. 7 E–E' seismic profile across the Aqia fault belt (see location in Fig. 2)

of Neogene. The right, eastward-dipping normal fault, F1, cuts upward into the highest stratigraphic layer in all of the three normal faults in this profile and cuts downward, through the Pliocene (sediments between T2 and T3), into the Paleozoic. The T2 and T3 reflection surfaces are distinct. Therefore, F1 is the most suitable fault to calculate the growth index of the Late Cenozoic normal faults on the D–D' profile (Fig. 6B).

The thicknesses of the Kuqa Formation (Pliocene) on both sides of the F1 fault are equal (the fault displacements at T2 and T3 are equal). The growth index of Kuqa Formation is 1.00, indicating that the normal faulting has not yet begun in the Pliocene. The thickness of the middle-lower part of Quaternary on the throw side is larger than that on the uplift side, and the growth index is 1.06, indicating the normal fault activation. The fault does not cut into the upper part of the Quaternary, and the growth index is 1.00. The normal faulting ceased. From this growth index calculation, that normal faulting began from Early Quaternary, lasted to mid-Quaternary, and then ceased in the Late Quaternary.

The E–E' profile is located south of the D–D' profile (Figs. 2, 7). Eight Late Cenozoic normal faults were revealed on it. The left four faults dip ENE and form staircase-like cross sections. The right four faults form small graben and horst structures. The normal faults cut through T2 upward into the Quaternary and downward into the Paleozoic. The fault displacement of the T2 is consistent with that below T2, indicating no these normal faulting before T2. The right two normal faults cut upward to Ta, a seismic reflection surface in the upper part of Quaternary. This is also the highest layer reached by the normal faults, indicating that the normal faulting ceased in the Late Quaternary.

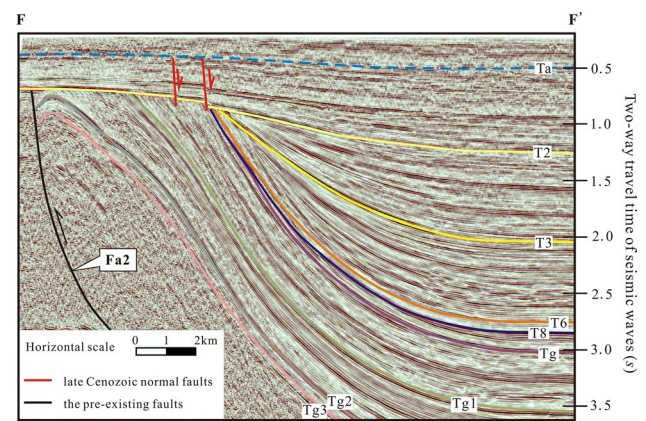


Fig. 8 F–F' seismic profile across the Aqia fault belt (see location in Fig. 2)

F–F' is a 2D seismic profile across the southern segment of the Aqia belt (Figs. 2, 8). Only two small normal faults were revealed on this profile. The Quaternary overlaps directly on the Paleozoic anticline, forming a large hiatus. The normal faults were revealed on the top of the Paleozoic anticline. They cut through T2 downward into the Paleozoic and upward into the Quaternary. The normal faults' displacements decrease upward from T2 and finally cease at Ta, which is a seismic reflection surface in the Middle–Upper Quaternary deposits. This indicates that the Late Cenozoic normal faulting seen in this profile ceased in Late Quaternary.

Late Cenozoic normal faults revealed on the Tumuxiuke belt

Late Cenozoic normal faults in the Tumuxiuke belt were revealed on its middle segment and on its uplift side (Figs. 2, 9, 10, 11).

G–G' is a 2D seismic profile across the mid-western segment of the Tumuxiuke belt (Figs. 2, 9). Four Late Cenozoic normal faults were revealed on this profile. They are grouped into an asymmetric graben. On the top of the Paleozoic anticline, the Quaternary directly overlaps the Permian, forming a huge hiatus. Laterally, the Kuqa Formation is cut by T2, suggesting that the anticline was deformed before the faulting affecting T2. The Late Cenozoic normal faults cut through the T2 reflection surface, downward into the Paleozoic layers and upward into the Quaternary deposits. The upmost reflection surface reached by the normal faults is Ta in the Middle–Upper Quaternary.

Figure 9B is the growth index diagram of F1. The fault displacements of the T2 reflection surface and those below it (in the Paleozoic) are equal. The thicknesses of the Carboniferous, Lower–Middle Permian, and Upper

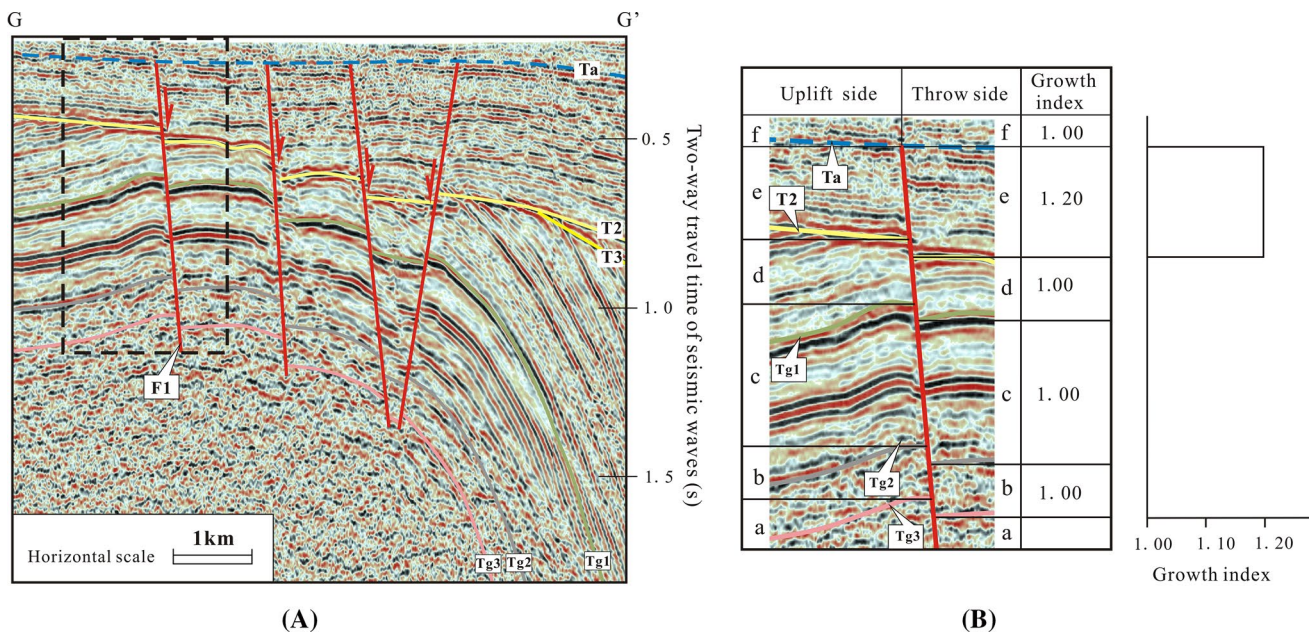


Fig. 9 G–G' seismic profile across the Tumuxiuke fault belt (see location in Fig. 2). **A** Seismic profile, **B** growth indices of the F1 fault: (a) pre-Carboniferous; (b) Carboniferous; (c) Middle and Lower Permian; (d) Upper Permian; (e) Middle and Lower Quaternary; (f) Upper Quaternary

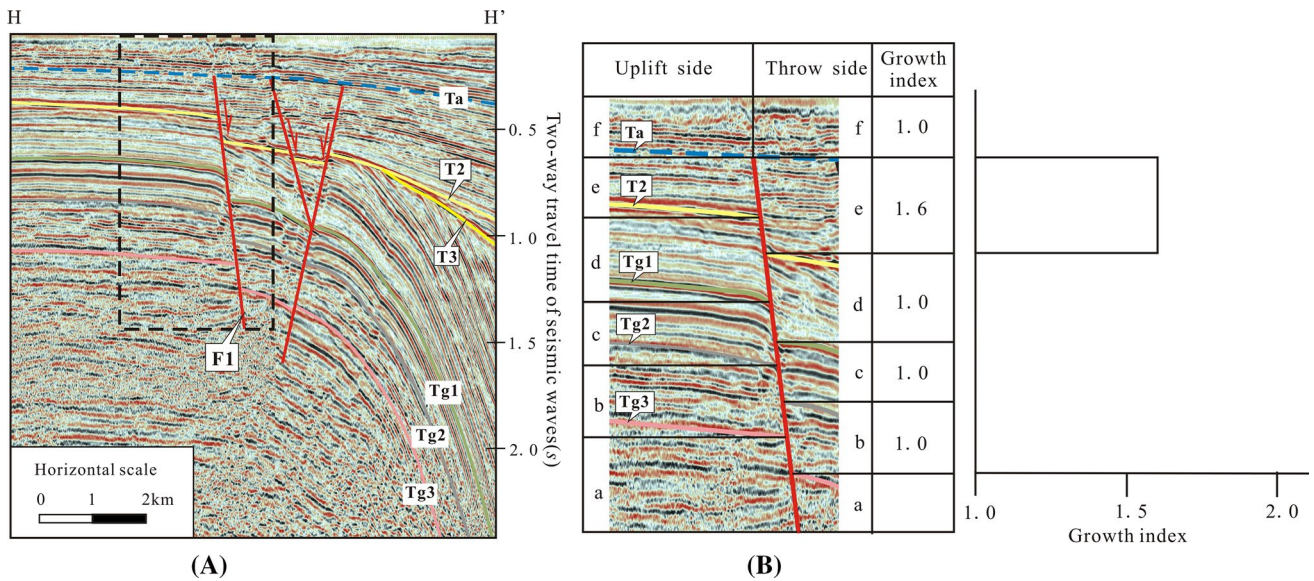


Fig. 10 H–H' seismic profile across the Tumuxiuke fault belt (see location in Fig. 2). **A** Seismic profile, **B** growth indices of the F1 fault: (a) pre-Carboniferous; (b) Carboniferous; (c) Lower–Middle Permian; (d) Upper Permian; (e) lower part of Quaternary; (f) upper part of Quaternary

Permian deposits on both sides of the fault are equal, and the growth indices are 1.00, indicating that the normal faulting had not yet begun. The normal fault displacements decrease gradually upward from T2 and died out at Ta. The thickness between T2 and Ta on the throw side is much larger than that on the uplift side, and the growth index is 1.20, representing the active period of the normal faults. The fault does not cut into the upper part of

the Quaternary, so the growth index is 1.00, indicating that the normal faulting ceased. From this growth index analysis, we conclude that the normal faulting began in Early Quaternary, last to mid-Quaternary, and ceased in Late Quaternary.

Extending T2 unconformity rightward on Fig. 9A, T2 cut Pliocene (Kuqa Fm). This is another evidence for the onset of the normal faulting in Quaternary.

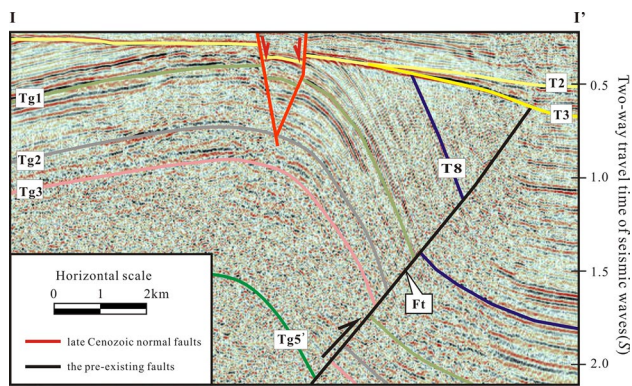


Fig. 11 I–I' seismic profile across the Tumuxiuke fault belt (see location in Fig. 2)

The H–H' 2D seismic profile is located in the middle segment of the Tumuxiuke fault belt, near the He4 well (Figs. 2, 10). The Late Cenozoic fault characteristics on H–H' are similar to those on G–G'. Three normal faults form a small, asymmetrical graben. The normal faults cut through T2, downward into the Paleozoic and upward into Quaternary. The normal faults in the Carboniferous–Permian are very distinct; however, they are less clear in the pre-Carboniferous due to poor seismic reflection. Ta in Middle–Upper Quaternary is the upmost reflection surface reached by the normal faults. We chose F1 for an example of growth index analysis (Fig. 10B).

All the growth indices calculated from the Carboniferous, Middle–Lower Permian, and Upper Permian are 1.00, suggesting that the normal faulting had not yet began in the Carboniferous and Permian. The growth index of the lower part of the Quaternary is 1.60, indicating normal faulting during that time. F1 cut not into the upper part of the Quaternary; the growth index there is 1.00, indicating that the normal faulting ceased.

I–I' is the easternmost 2D seismic profile on which Late Cenozoic normal faults were revealed (Figs. 2, 11). 2 Quaternary normal faults revealed on this profile dip toward each other forming a little graben.

Discussion on the origin of the Late Cenozoic normal faults discovered around the Awati Sag

After careful seismic interpretation and fault analysis, we can get the following basic characteristics of the Late Cenozoic normal faults revealed on the boundaries of Awati Sag. All the normal faults were distributed along Shajingzi, Aqia, and Tumuxiuke faults, the three preexisting basement-involved boundary faults between Awati and its neighboring blocks, indicating that the normal faulting was induced by the reactivation of the preexisting boundary faults. The

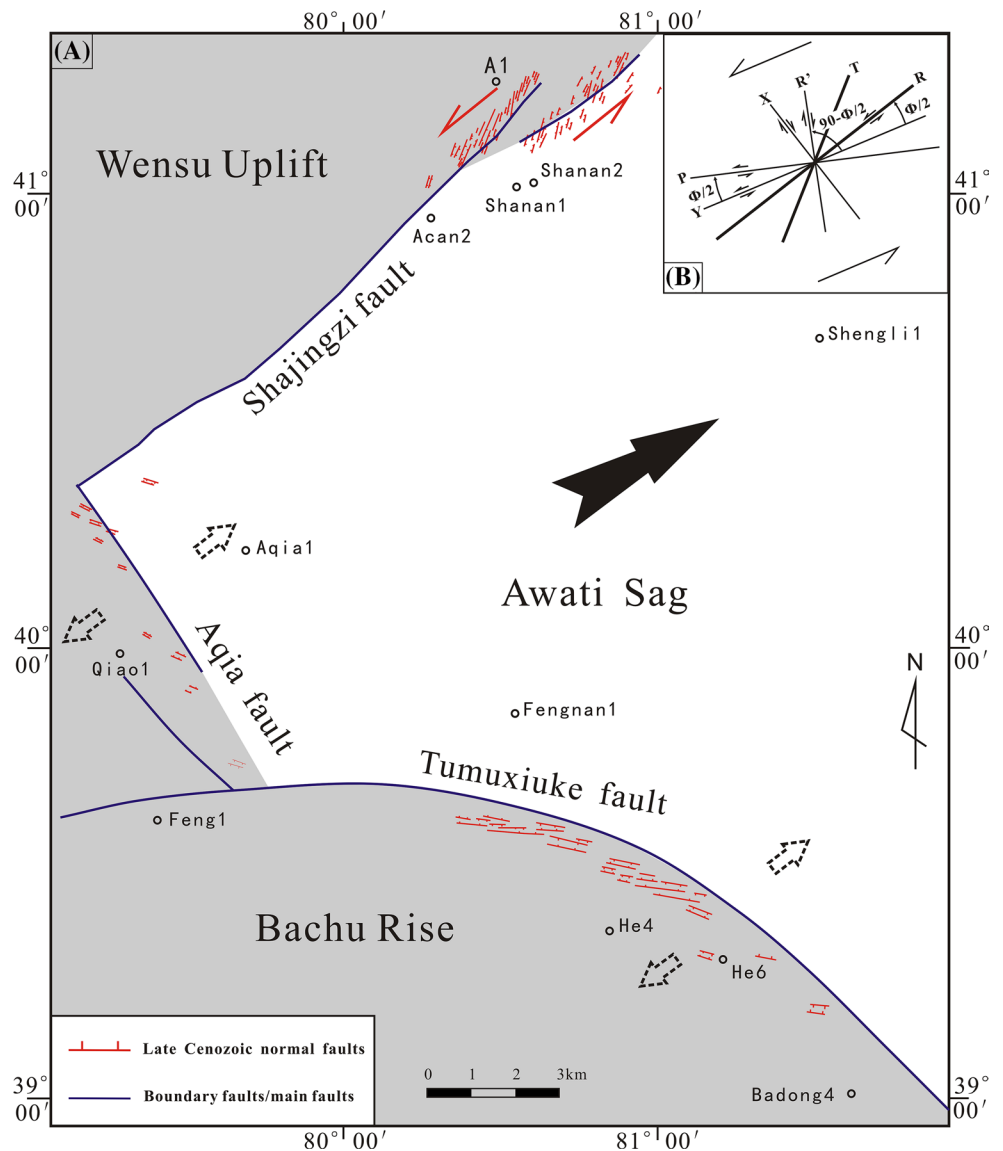
normal faults on the Shajingzi belt were arranged in right-step, en echelon pattern horizontally and combined into negative flower structure in profile, forming a Late Cenozoic transtensional fault belt. The normal faulting on Shajingzi began from Late Pliocene, last to mid-Quaternary, and then ceased in Late Quaternary. The normal faults on Aqia are similar to those on Tumuxiuke. They trend NW–SE, consistent with the Aqia and Tumuxiuke belts, and almost perpendicular to Shajingzi and the Late Cenozoic transtensional fault belt on it. The normal faults on Aqia and Tumuxiuke were combined into staircase pattern and graben–horst structure in profile showing the typical characteristics of tensional structure. The normal faulting began from Early Quaternary, last to mid-Quaternary, and then ceased. The beginning time of the normal faulting on Shajingzi is some earlier than those on Aqia and Tumuxiuke.

The Late Cenozoic normal faults on Shajingzi were arranged in en echelon pattern. This is common in strike-slip system (Tchalenko and Ambraseys 1970; Wilcox et al. 1973; Bartlett et al. 1981). The numerous small normal faults were arranged in en echelon pattern and form a transtensional fault belt. The direction of the belt is consistent with “R” plane in strike-slip system (Tchalenko and Ambraseys 1970; Bartlett et al. 1981). The direction of the normal faults is consistent with the “T” plane (Bartlett et al. 1981) (Fig. 12).

Late Pliocene–mid-Quaternary left-lateral strike-slip occurred first on Awati's NW boundary, forming Shajingzi transtensional fault belt, and then, due to the eastward escape of Awati block, a tensional stress on Awati's SW boundary developed the Quaternary normal faults on Aqia and Tumuxiuke belts (Fig. 12).

The previous study has identified four phases of obvious acceleration of mountain uplifting accompany with intense structural deformation in Tianshan and its adjacent area, those are 25–24 Ma (Avouac and Tapponnier 1993; Hendrix et al. 1994; Sobel and Dumitru 1997; Guo et al. 2006), 16–15 Ma (Windley et al. 1990; Allen et al. 1993), 11–10 Ma (Avouac and Tapponnier 1993; Charreau et al. 2006, 2009; Xiao et al. 2005a, b), and 5–0 Ma (Avouac and Tapponnier 1993; Zhang et al. 1996; Charreau et al. 2006, 2009; Guan et al. 2007). The transtensional faulting on Shajingzi and normal faulting on Aqia and Tumuxiuke are consistent with the last deformation phase (5–0 Ma) in Tianshan. And the preexisting Tumuxiuke, Aqia, and Shajingzi basement-involved boundary faults possibly represent the 11–10 Ma deformation (Qi et al. 2012; Liu et al. 2013). Charreau et al. (2009) advocated a young (<5 Ma) counterclockwise rotation in the Jingu River area, assigned to a left-lateral strike-slip in the northern piedmont. The Pliocene–Quaternary left-lateral strike-slip on Shajingzi belt exhibits a similar sinistral strike-slip took place on the southern side of Tianshan.

Fig. 12 Genesis of the Late Cenozoic transensional normal fault belts around the Awati Sag. *Boxed insert (b)* illustrates orientations and sense of shear for R-, R', P-, X- and Y-shears and T fracture in the left-lateral shear zone (modified after Bartlett et al. 1981)



Conclusion

1. Late Cenozoic normal faults were developed around the Awati Sag. They were distributed along the pre-existing, basement-involved boundary faults, i.e., the Shajingzi, Aqia, and Tumuxiuke faults, indicating that the normal faulting was induced by the reactivation of the boundary faults.
2. The Late Cenozoic normal faults on Shajingzi belt are arranged into right-step, en echelon pattern and grouped into small negative flower structures, forming a right-step, sinistral transensional fault belt. The Late Cenozoic normal faults on Aqia and Tumuxiuke belts are parallel to each other horizontally and grouped into staircase pattern and graben and horst structures, showing the typical characteristics of tensional structure.

3. The Late Cenozoic normal faulting on Shajingzi belt began from Late Pliocene, last to mid-Quaternary, and then ceased. Those on Aqia and Tumuxiuke began from Early Quaternary, last to mid-Quaternary, and then ceased. The beginning time of the Late Cenozoic normal faulting on Aqia and Tumuxiuke is some later than that on Shajingzi.
4. Late Cenozoic left-lateral strike-slip occurred first on Awati's NW boundary, forming Late Pliocene–mid-Quaternary Shajingzi transensional fault belt. And then, due to the eastward escape of Awati block, a tensional stress on Awati's SW boundary developed the Quaternary normal faults on Aqia and Tumuxiuke belts. The Late Pliocene–mid-Quaternary left-lateral strike-slip on Shajingzi belt is consistent with the similar sinistral strike-slip in the northern piedmont of Tianshan (Charreau et al. 2009).

Acknowledgments We express our great appreciation to Prof. Jacques Charvet and other anonymous reviewer for their constructive comments that significantly improved the quality of the manuscript. Gratitude is expressed to Tarim Oilfield Company, PetroChina for providing us with valuable seismic data. We are thankful to Prof. Yi-Xiong Qian, Dao-Xuan Wang and Dr. Yue-Ran Wang for the beneficial discussions we had with them. This study is financially supported by the Key National Science and Technology Specific Projects (2011ZX05028-003-02) and Science and Technology Programs of Tarim Oilfield Company, PetroChina.

References

- Allen MB, Windley BF, Zhang C, Guo J (1993) Evolution of the Turfan basin, Chinese central Asia. *Tectonics* 12:889–896
- Allen MB, Vincent SJ, Wheeler PJ (1999) Late Cenozoic tectonics of the Kepingtage thrust zone: interactions of the Tien Shan and Tarim Basin, northwest China. *Tectonics* 18:639–654
- Avouac J-P, Tapponnier P (1993) Kinematic model of active deformation in Central Asia. *Geophys Res Lett* 20:895–898
- Bartlett WL, Friedman M, Logan JM (1981) Experimental folding and faulting of rocks under confining pressure. *Tectonophysics* 79:255–277
- Charreau J, Gilder S, Chen Y, Dominguez S, Avouac J-P, Sen S, Jolivet M, Li Y, Wang W (2006) Magnetostratigraphy of the Yaha section, Tarim Basin (China): 11 Ma acceleration in erosion and uplift of the Tian Shan mountains. *Geology* 34:157–160
- Charreau J, Chen Y, Gilder S, Barrier L, Dominguez S, Augier R, Sen S, Avouac J-P, Gallaud A, Graveleau F, Wang Q (2009) Neogene uplift of the Tian Shan Mountains observed in the magnetic record of the Jingou River section (northwest China). *Tectonics*. doi:10.1029/2007TC002137
- Chen HL, Luo JC, Guo QY, Liao L, Xiao ZY, Cheng XG, Yang SF, Wang BQ (2009) Deformation history and tectonic evolution of Southeastern Tarim Basin in Mesozoic and Cenozoic. *Geotecton Metallog* 33(1):38–45 (in Chinese with English abstract)
- Guan SW, Li BL, He DF, Wang X, Suppe J, Lei GL (2007) Late Cenozoic active fold-and-thrust belts in the southern and northern flanks of Tianshan. *Acta Geol Sinica* 81(6):725–744 (in Chinese with English abstract)
- Guo LZ, Shi YS, Lu HF (1992) Two kinds of long distance effect by collision of Indian and Qingzang tectonic plates. In: Li QB, Dai JX, Liu RQ, Li JL (eds) Symposium of the researches on modern geology, vol 1. Nanjing University Press, Nanjing, pp 1–8 (in Chinese)
- Guo Z, Zhang Z, Wu C, Fang S, Zhang R (2006) The Mesozoic and Cenozoic exhumation history of Tianshan and comparative to the Junggar and Altai Mountains. *Acta Geol Sinica* 80(1):1–15 (in Chinese with English abstract)
- Hendrix MS, Dumitru TA, Graham SA (1994) Late Oligocene-early Miocene unroofing in the Chinese Tianshan: an early effect of the India-Asia collision. *Geology* 22:487–490
- Jia CZ, Yao HJ, Gao J, Zhou DY, Wei GQ (1992) Stratigraphic system of the Tarim Basin. In: Tong XG, Liang DG (eds) Symposium of the oil and gas exploration in the Tarim Basin. Xinjiang Technology and Medical Publishing House, Urumqi, pp 34–63 (in Chinese)
- Jia CZ, Yang SF, Chen HL, Wei GQ (2001) Structural geology and natural gas of the group of basins in the northern margin of Tethyses. Petroleum Industry Press, Beijing, pp 1–162 (in Chinese)
- Jia CZ, Zhang SB, Wu SZ (2004) Stratigraphy of the Tarim Basin and adjacent areas. Science Press, Beijing, pp 1–547 (in Chinese)
- Li HH, Zhou DY, Feng Q, Zou DP (1992) The establishment of seismic stratigraphic sequence in Eastern Tarim Basin. In: Tong XG, Liang DG (eds) Symposium of the oil and gas exploration in Tarim Basin. Xinjiang Technology and Medical Publishing House, Urumqi, pp 142–157 (in Chinese)
- Li YJ, Song WJ, Mai GR, Zhou LX, Hu JF, Shang XL (2001) Kuqa foreland basin, Northern Tarim foreland basin and their coupling relationship. *Xinjiang Pet Geol* 22(5):376–381 (in Chinese with English abstract)
- Li YJ, Zhao Y, Sun LD, Song WJ, Zheng DM, Liu YL, Wang DX, Hu JF, Zhang QR (2013) Meso-Cenozoic extensional structures in the northern Tarim Basin, NW China. *Int J Earth Sci* 102(4):1029–1043
- Liu YL, Li YJ, Qi YM, Hu XF, Shen YM, Wang YR, Liu LW, Chen YG, Zhao Y (2013) Fault analysis on Tumuxiuke fault belt, Tarim Basin, NW China. *Chin J Geol* 48(1):124–132 (in Chinese with English abstract)
- Lu HF, Howell DG, Jia D (1994) Kalpin transpression tectonics, northwestern Tarim basin, western China. *Int Geol Rev* 36:975–981
- Lu HF, Chen CM, Liu ZH, Jia D, Wang GQ, Jia CZ (2000) The structural features and origin of the Kuqa rejuvenation foreland thrust belt. *Acta Pet Sin* 21(3):19–24 (in Chinese with English abstract)
- Molnar P, Tapponnier P (1975) Cenozoic tectonics of Asia: effects of a continental collision. *Science* 189(4201):419–426
- Qi YM, Li YJ, Wang YR, Liu YL, Zhu HY, Liu LW, Mo T, Chen YG (2012) Fault analysis on Shajingzi structural belt, NW margin of Tarim Basin, NW China. *Chin J Geol* 47(2):265–277 (in Chinese with English abstract)
- Scharer KM, Burbank DW, Chen J (2004) Detachment folding in the Southwestern Tian Shan–Tarim foreland, China: shortening estimates and rates. *J Struct Geol* 26:2119–2137
- Shu LS, Wang B, Yang F, Lu HF, Charvet J, Laurent-Charvet S (2003) Polyphase tectonic events and Cenozoic basin-range coupling in the Tianshan belt, northwestern China. *Acta Geol Sinica* 77(4):457–467
- Sobel ER, Dumitru TA (1997) Thrusting and exhumation around the margins of the western Tarim basin during India-Asia collision. *J Geophys Res* 102:5043–5063
- Sun LD, Li YJ, Song WJ, Tian ZJ, Wang GL, Wu GH (2002) Tectonics and oil–gas distribution in the North Tarim Basin, NW China. *Chin J Geol* 37(Suppl):1–13 (in Chinese with English abstract)
- Tang LJ, Jin ZJ (2000) Negative inversion process and hydrocarbon accumulation of Yaha Fault Belt in Northern Uplift, Tarim Basin. *Acta Sedimentol Sin* 18(2):302–309 (in Chinese with English abstract)
- Tang LJ, Jin ZJ, Zhang YW, Lu KZ (1999) Negative inversion structures and geological significance of Northern Uplift, the Tarim Basin, Northwestern China. *Geosciences* 13(1):93–98 (in Chinese with English abstract)
- Tang LJ, Jin ZJ, Jia CZ, Pi XJ, Chen SP, Xie HW, Wang ZY (2004) A large-scale salt nappe complex in the leading edge of the Kuqa foreland fold-thrust belt, Tarim Basin, Northwest China. *Acta Geol Sin* 43(2):17–25 (in Chinese with English abstract)
- Tapponnier P, Molnar P (1977) Active faulting and tectonics in China. *J Geophys Res* 82:2905–2930
- Tapponnier P, Peltzer G, Armijo R (1986) On the mechanics of the collision between India and Asia. In: Coward MP, Ries AC (eds) Collision tectonics. Geological Society Special Publication No. 19, pp 115–157
- Tchalenko JS, Ambraseys NN (1970) Structural analysis of the Dasht-e Bayaz (Iran) earthquake fractures. *Geol Soc Am Bull* 81:41–60
- Wang RD (1992) New progress of seismic geologic stratum division and calibration in Tarim Basin. In: Tong XG, Liang DG (eds) Symposium of the oil and gas exploration in Tarim Basin. Xinjiang technology and medical publishing house, Urumqi, pp 131–141 (in Chinese)
- Wang GL, Li YJ, Sun JH, Huang ZB, Zhao Y, Liu YL (2009) Structural deformation characteristics of the Kalpin thrust belt, NW

- Tarim. *Chin J Geol* 44(1):50–62 (in Chinese with English abstract)
- Wei GQ, Jia CZ, Shi YS, Lu HF, Li YH (2001) Tectonic characteristics and petroleum accumulation in extensional-shear fault system in Mesozoic-Cenozoic formations in the northern area of Tabei Uplift, Tarim. *Acta Pet Sin* 22(1):19–24 (in Chinese with English abstract)
- Wilcox RE, Harding TP, Seely DR (1973) Basic wrench tectonics. *Am Assoc Pet Geol Bull* 57(1):74–96
- Windley BF, Allen MB, Zhang C, Zhao ZY, Wang GR (1990) Paleozoic accretion and Cenozoic deformation of the Chinese Tien Shan Range, central Asia. *Geology* 18:128–131
- Xiao AC, Yang SF, Li YJ, Wang QH, Chen HL (2005a) A study of Cenozoic fracture in Bachu-Kalpin area, Tarim Basin. *Oil Gas Geol* 26(1):78–86 (in Chinese with English abstract)
- Xiao AC, Yang SF, Li YJ, Wang QH, Chen HL, Cheng XG (2005b) Main period for creation of fracture system in the Bachu Uplift, Tarim Basin. *Chin J Geol* 40(2):291–302 (in Chinese with English abstract)
- Yang HJ, Li YJ, Shi J, Xiao AC, Huang SY, Wu GY, Wang HS, Wang X, Zhao Y, Liu YL (2010) Tectonic characteristics of the late Cenozoic South Tianshan fold-thrust belt. *Quat Sci* 30(5):1030–1043 (in Chinese with English abstract)
- Zhang PZ, Deng QD, Yang XP, Peng SZ, Xu XW, Feng XY (1996) Late Cenozoic tectonic deformation and mechanism along the Tianshan Mountain, Northwestern China. *Earthq Res China* 12(2):127–140 (in Chinese with English abstract)
- Zhang PD, Huang TZ, Ding Y (1999) Major negative reverse fractures and their control over petroleum in the north of Shaya Uplift, Tarim Basin. *Pet Geol Eng (Henan Pet)* 13(6):7–13 (in Chinese)
- Zhang SB, Huang ZB, Zhu HC (2004) Phanerozoic strata in cover area of Tarim Basin, Xinjiang. Petroleum Industry Press, Beijing, pp 151–189 (in Chinese with English abstract)
- Zhao Y, Li YJ, Sun LD, Zheng DM, Liu YL, Wang DX, Wei HX, Guan WS (2012) Mesozoic-Cenozoic extensional structure in North uplift of Tarim basin and its genetic discussion. *Acta Pet Sin* 28(8):2557–2568 (in Chinese with English abstract)